CrossMark

ORIGINAL ARTICLE

Photodegradation of odorous 2-mercaptobenzoxazole through zinc oxide/hydroxyapatite nanocomposite

F. Buazar · S. Alipouryan · F. Kroushawi ·
S. A. Hossieni

Abstract In this study, ZnO/HAP nanocomposite with excellent photocatalytic activities was successfully synthesized by sol–gel method and used for degradation of 2-mercaptobenzoxazole (MBO) as model of odorous mercaptan compound in water. To optimize the performance of ZnO/HAP photocatalytic capabilities, ZnO/HAP loading (0.05–0.3 g/L), irradiation time (15–180 min), pH (3–11) and initial concentration of MBO (10–100 ppm) were investigated. At neutral pH of 7, the highest amount of the MBO (99.45 %) was degraded by ZnO/HAP nanocomposite through photocatalytic oxidation process within 2 h of irradiation time. A maximum adsorption capacity of 197.64 mg g^{-1} was obtained for ZnO/HAP under optimized conditions. BET results indicated that ZnO/HAP had a surface area of 182.36 mg^{2}g^{-1} which was much greater than pure ZnO nanoparticles (31.2 mg^{2}g^{-1}). TEM image demonstrated a spherical shape structure of ZnO/HAP with average particle size of 25 nm in diameter. The XRD patterns revealed the principal components of ZnO/HAP including HAP and ZnO. FTIR spectrum results supported formation ZnO and HAP by their stretching mode in composite. Comparison of photocatalytic activity of ZnO/HAP with pure ZnO and HAP nanoparticles had clearly recognized that latter is the most active photocatalyst in the degradation of MBO using UV light as source energy. The reason for greater activity of ZnO/HAP was due to its larger specific surface area (182.36 m^{2}g^{-1}) and high generation of active HO$^{\cdot}$ and O$_2^{-2\cdot}$ species.

F. Buazar (✉)
Department of Marine Chemistry, Khoramshahr
University of Marine Science and Technology,
P.O. Box 669, Khoramshahr, Iran
e-mail: f.buazar1979@gmail.com

F. Buazar · S. Alipouryan
Nanotechnology Research Centre, Ahvaz Jundishapur University
of Medical Sciences, P.O. Box 61357–33184, Ahvaz, Iran

F. Kroushawi
Department of Energy Conversion and Storage, Technical
University of Denmark, Risø Campus, Frederiksborgvej 399,
Building 779, 4000 Roskilde, Denmark

F. Kroushawi
Department of Physics, Vali-e-Asr University of Rafsanjan,
P.O. Box 518, Rafsanjan, Iran

S. A. Hossieni
Nutrition and Metabolic Diseases Research Center, Ahvaz
Jundishapur University of Medical Sciences, Ahvaz, Iran

Introduction

Mercaptans are unpleasant odorous organosulfur pollutants which are produced by the wood-pulping industry, manure and sewer systems as exhaust gases in natural environments (Greyson 1990; Leh and Chan 1973). Environmental Protection Agency of United States (EPA) estimates that over 450 tons of mercaptan may be lost annually into the environment with great impact on human health. So removal of organosulfur compounds from aqueous solution has been one of the major investigations in the last decades (Habibi and Sheibani 2012). Among them, the pollution of the environment by 2-mercaptobenzoxazole (MBO) is always of great concern for aquatic organisms. MBO is widely used in industries as rubber vulcanization or corrosion inhibitor (Allaouia and Wong-Wah-Chung 2010). Some studies on the

environmental behavior and the biodegradation of MBO indicated that in environmental conditions it is very stable and cannot completely mineralized (Allaouia and Wong-Wah-Chung 2010; Habibi and Sheibani 2012). To the best of our knowledge, very few works were reported specifically on the removal of MBO (Antonopoulou et al. 2014; Habibi and Sheibani 2010; Parham and Khoshnam 2013). Hence, in aspect of established toxicity, low biodegradability and persistence of MBO in natural compartments, further work on its elimination and/or mineralization needs to be addressed.

ZnO nanoparticles (Nps) is well-known photocatalyst (Chong et al. 2010; Georgekutty et al. 2008; Hariharan 2006) for the degradation of several environmental contaminants due to its chemical inert, high photosensitivity, high electron mobility, stability, large band gap (3.37 eV) and non-toxic properties (Bahnemann 1991; Deng et al. 2008; Yusoff et al. 2014). Likewise, ZnO Nps are identified as the most promising sorbent due to their high metal uptake (Ali 2012; Mahdavi et al. 2012; Mohammad Vaseem and Hahn 2010; Sheela et al. 2012). Since the photocatalytic reaction occurs on the surface of ZnO Nps, its photocatalytic activity can increase through immobilization of the catalyst onto a substrate that improves its surface properties (Bai et al. 2013; Saravanan et al. 2013).

In this connection, hydroxyapatite (HAP), with nominal composition $Ca_{10}(PO_4)_6(OH)_2$, can be considered as valuable candidate for supporting material due to its bio-compatibility and excellent adsorption properties toward diverse water pollutants (Azzaoui et al. 2014; Hokkanen et al. 2014). Meanwhile, HAP was recognized for its high potential in trapping and retention of toxic heavy metals (Liu et al. 2013; Xie et al. 2013; Zhao et al. 2014b) and photocatalytic decomposition of toxic organic materials (Bouyarmane et al. 2013; Wei et al. 2014) in polluted water. Yet, no report has been published on removal of organic MBO pollutant from water via ZnO/HAP nanophotocatalyst. So, following our pervious studies on synthesis of Nps (Buazar et al. 2012; Kassaee and Buazar 2009; Kassaee et al. 2008), in this paper, ZnO/HAP nanocomposite was synthesized using simple and cost-effective sol–gel procedure. The effect of parameters such as ZnO/HAP doses, initial concentration of MBO, irradiation time and pH were investigated on the photooxidation of MBO in water under UV irradiation. Owing to the adsorption properties of HAP and the photocatalytic properties of ZnO, the results demonstrated that photodecomposition of MBO on ZnO/HAP surface was much faster than pure ZnO and HAP Nps.

Materials and methods

Materials

Zinc acetate dihydrate $(Zn(CH_3COO)_2 \cdot 2H_2O)$ (99.99 %,w/w), 2-propanol (C_3H_7OH) (99.99 %,w/w), pure ethanol (CH_3CH_2OH), 2-aminoethanol (MEA, C_2H_7NO), calcium nitrate $(Ca(NO_3)_2.4H_2O)$ and di-ammonium hydrogen phosphate $((NH_4)_2HPO_4)$ were of analytical grade and purchased from Merck (Darmstadt, Germany). 2-Mercaptobenzoxazole (CAS No. 2382-96-9, Fluka, Swiss) is used as organic pollutant (Fig. 1). Deionized (DI) water is used for rinsing and for makeup of all aqueous solutions.

Sol–gel synthesis of ZnO/HAP nanocomposite

ZnO/HAP nanopowder was synthesized using the sol–gel technique (Hayat et al. 2011). Typically, appropriate amount of zinc acetate (0.018 mol) is solved in 20 mL of 2-propanol for 1 h, then 20 mL of MEA was added to a solution of zinc acetate. Sol was stirred in hot water bath at 65 °C for 1 h, then water was added drop-wise to the above solution under vigorous mechanical stirring (1,400 rpm) for 10 min. The white precipitate was produced instantly. Separately, mixture solution consisting of 0.034 mol $(Ca(NO_3)_2.4H_2O)$ and 0.023 mol $(NH_4)_2HPO_4$ with pH adjusted to 11 were added drop-wise to the obtained precipitate solution within 30 min. The resulting white suspension was heated at 90 °C for 1 h and then the sol mixture was aged for 24 h without stirring. The obtained precipitate was washed several times with ID water then dried in an oven at 90 °C for 3 h and finally ground with mortar.

Characterization of ZnO/HAP

The morphology and size of the synthesized ZnO/HAP nanocomposite were probed on Leo 912 AB transition electron microscope (TEM) at an accelerating voltage of 120 kV. Infrared spectra of chemical compositions of as prepared ZnO/HAP nanocomposite were recorded on Fourier transform infrared spectroscopy (FTIR, Brucker Tensor 27) spectrometer using a KBr wafer. Crystal structure and the size of nanocomposite were obtained from X-ray diffraction (XRD) on a Xpret Pro-Philips diffractometer with CuK $(\lambda = 1.5405$ Å) radiation at a scanning speed of 2/min from 10 to 80 (2θ). The Brunauer–Emmett–Teller (BET) specific surface area of the synthesized materials is determined by nitrogen adsorption–desorption at 77.30 K using an ASAP2450 apparatus.

Photocatalytic experiments

The photodegradation procedure of MBO was conducted in a photoreactor (Fig. 2). Firstly, 25 mL sample of wastewater containing 20 ppm of MBO and 10 mg of ZnO/HAP Nps with the initial pH of 4 was prepared and kept in the darkness for 30 min. Afterward, the prepared mixture was exposed to UV irradiation using UV lamps under

Fig. 1 Physical state and structure of 2-mercaptobenzoxazole (MBO), $\lambda_{max} = 294$ nm, molecule weight ($Mw = 151.19$ gmol^{-1})
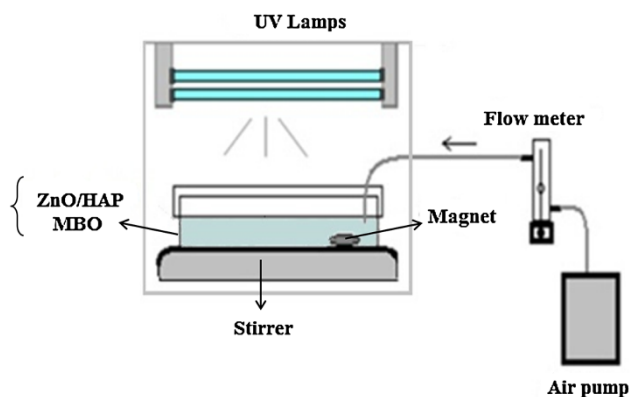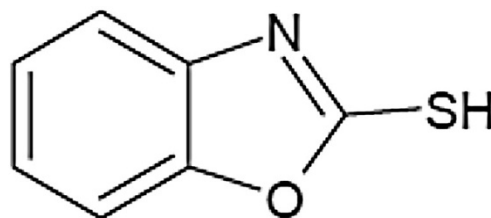
Fig. 2 Schematic representation of the UV photoreactor equipments

continuous stirring (500 rpm) at room temperature (25 °C). The engaged UV lamps were two 8 W low-pressure mercury lamps (Philips, $\lambda = 365$ nm) which were placed 5 cm above a jar containing the polluted water. All photodegradation experiments were conducted in a batch reactor. After illumination for different times (8 samples, see Fig. 7), the suspension is sampled and the degradation process of MBO is monitored by UV/Vis absorbance. To ensure repeatability, three trials of degradation of MBO were done for each experiment. According to the change in the concentration of MBO, The removal percentage (%R) of MBO versus time is defined as Eq. 1:

$$\%R = \left(\frac{C_0 - C_t}{C_0} \right) \times 100 \tag{1}$$

where C_o is the initial concentration of MBO, C_t is the concentration of MBO at certain reaction time t (min).

Results and discussion

Characterization of ZnO/HAP nanocomposite

FTIR analysis

FTIR spectroscopy is useful technique to prove formation of the ZnO/HAP Nps. Analysis of ZnO/HAP by FTIR demonstrated that all characteristic bands of ZnO and HAP appeared in the IR spectrum. For example, characteristic peaks of O–H bending at 23,600 cm^{-1}, O–H stretching at

3,386 and stretching mode of PO_4^{-3} groups at 1,050 and 1,348 cm^{-1} (Amer et al. 2014). Moreover, the new band at 570 cm^{-1} could be attributed to the adsorption peak of ZnO species in ZnO/HAP nanocomposite (Fig. 3) (Zhang et al. 2011).

XRD

XRD patterns of ZnO/HAP nanocomposite revealed principal components of HAP and ZnO (Fig. 4a). According to the XRD pattern no impurities could be found in the particles confirming that the product was exclusively ZnO/HAP composite. The crystallinity of the HAP was confirmed by the reflections observed at typical 2θ values of 25.87°, 31.76°, 39.8°, 46.6° and 49.5° (JCPDS cards No. 74-565) (Zhao et al. 2014a). Meanwhile, the main peaks at 36.60° (101), 47.65° (102) and 62.70 (103) were attributed to hexagonal structure of ZnO Nps (JCPDS cards No. 89-0510). The particles diameter is determined from the diffraction peak broadening using Scherrer's equation (Birks and Friedman 2004):

$$D = K\lambda/COS\theta \tag{2}$$

where D is the crystal size of the Nps, the value of the coefficient K is 0.90, θ (radian) is the diffraction angle, λ is the X-ray wavelength (1.5405 Å), and β is the width of XRD peak at half height. The average crystallite size of ZnO and HAP according to the most intensive diffraction peak at $2\theta = 25.87°$ and $2\theta = 36.60°$ are 12 ± 1.2 and 20 ± 1.2 nm, respectively (Fig. 2). These results were consistent with the IR observations (Fig. 3)

TEM analysis

TEM image clearly indicated that the synthesized ZnO/HAP Nps appeared rather monodisperse and have an average size of about 25 nm in diameter. Moreover, it consists of less agglomeration of spherical particles, confirming the formation of nanocomposite which is important for further advanced applications (Fig. 4b). Probably, HAP makes a shell layer around ZnO particles to avoid its growth and retains a stable dispersion compared to those without any protection (Giannakopoulou et al. 2012).

Fig. 3 FTIR spectrum of prepared ZnO/HAP nanocomposite
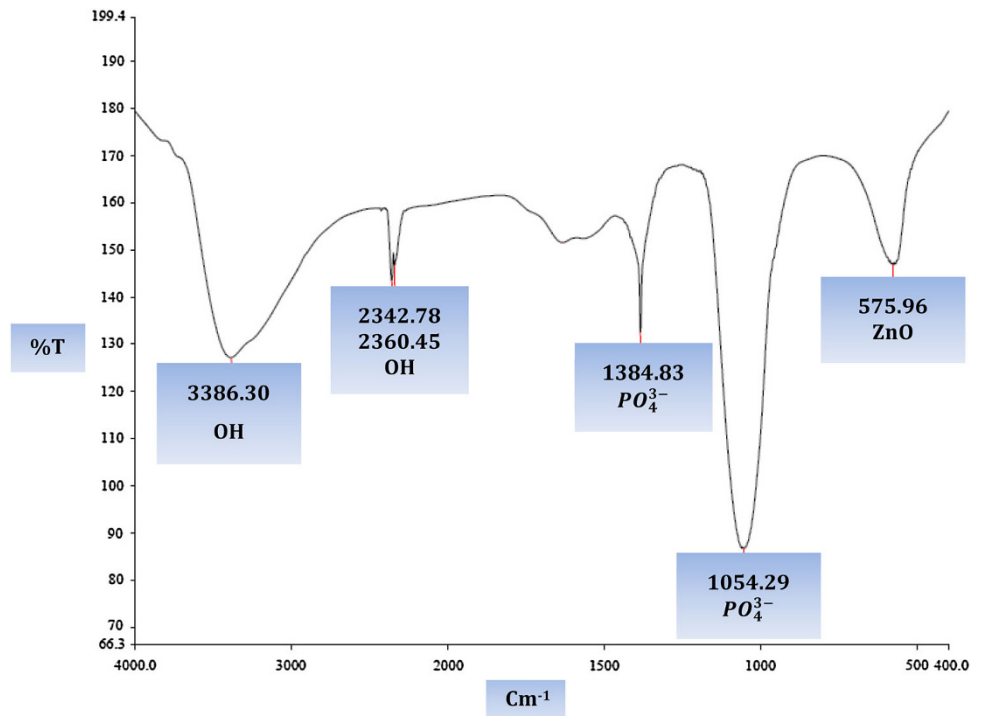
BET analysis

According to BET results, ZnO/HAP nanostructure demonstrated the isotherm of type IV, with a hysteresis loop at relative pressure ($P/P\circ$) between 0.4 and 1.0, showing the existence of mesoporous structures (Fig. 5) (Mohamed and Aazam 2013). Meanwhile, the calculated values for ZnO/HAP nanocomposite including BET specific surface area (SSA, 182.36 mg^{2}g^{-1}), total pore volume (0.0329 cm^{3}g^{-1}) and mean pore diameter (7.182 nm) indicated that our nanocomposite has a much greater surface area than pure ZnO Nps (31.2 nm) (Table 1). These results confirmed TEM and XRD findings (Figs. 5, 4). Consequently, higher specific surface areas and porous structures of ZnO/HAP nanophotocatalyst enhanced its photocatalytic performance toward organic MBO pollutant rather than pure ZnO Nps (Tables 1, 2) (Giannakopoulou et al. 2012). Moreover, SSA of ZnO/HAP was greater than other reported catalysts in literature (Sakthivel et al. 2003), indicating its higher photocatalytic activity.

Effect of pH

The effect of solution pH on the photocatalytic performance of the ZnO/HAP nanoadsorbent was detected in the initial pH range of 3–11. The degradation efficiency of MBO increased first and then decreased slightly with rising pH from 8 to 11 (Fig. 6a). The photocatalytic degradation of MBO reaches maximum at neutral pH = 7. The impact of pH on the adsorption capacity of the ZnO/HAP can be

explained on the basis of the point of zero charge of ZnO and proton concentration (Sakthivel et al. 2003). The point of zero charge of ZnO was reported as 9.0 (Neppolian et al. 1998). At alkaline condition (pH > 9), with the decrease of number of protons in the solution there are not enough protons to trap photo-electrons, which could restrain the production of hydroxyl groups. Subsequently, the nanoadsorbent affinity toward MBO becomes weak gradually. In contrast, at lower pH < 9, electrostatic interactions between MBO anions and the positive catalyst surface lead to strong adsorption of the former on the ZnO/HAP catalyst (Sakthivel et al. 2003).

Design of experiments and statistical analysis

A series of experiments were carried out to understand the effects of various operating parameters on the degradation of MBO and to find out the most influential parameters affecting the process. Based on the single factor study, three parameters—photocatalyst dose, initial concentration of MBO and pH—were found to influence the reaction most. The Box–Behnken design of experiment method, which has been used along with RSM for the optimization of various experimental processes, was used to design the experiments required for the optimization (Zhang et al. 2010). The ranges and levels of independent variables considered in the design are shown in Table 3. The experimental results were fitted to a quadratic polynomial model for three parameters represented by Eq. 1.
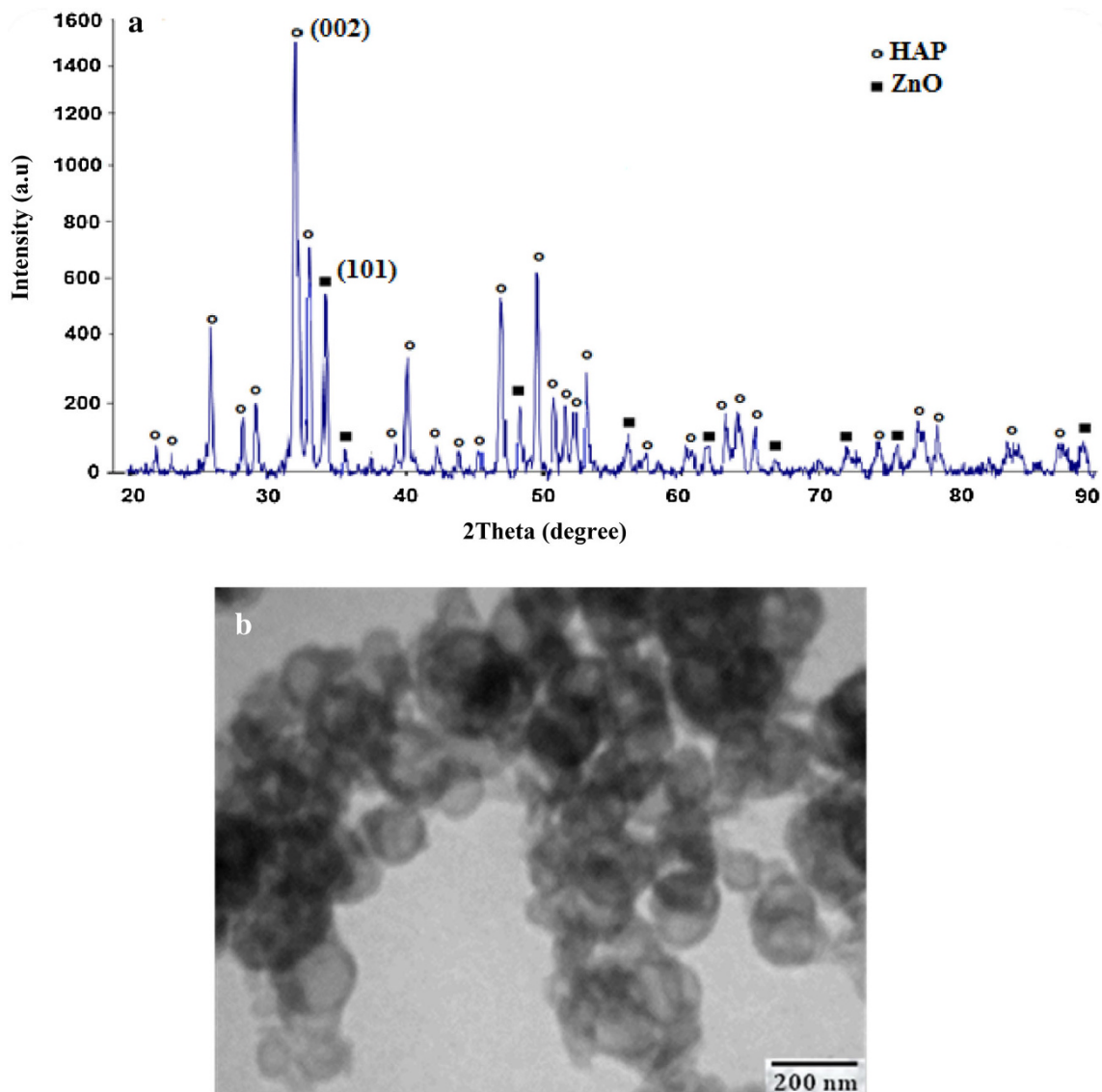
Fig. 4 **a** XRD pattern and **b** TEM micrograph of the ZnO/HAP nanocomposite recorded at 20,000 magnifications

$$Y = \beta_1 A + \beta_2 B + \beta_3 C + \beta_{11} A^2 + \beta_{22} B^2 + \beta_{33} C^2 + \beta_{12} AB + \beta_{23} BC + \beta_{31} CA \qquad (1)$$

where, Y represents the response variable, $\beta_1, \beta_2, \beta_3$ the coefficients of the independent variables, $\beta_{11}, \beta_{22}, \beta_{33}$ quadratic coefficients, $\beta_{12}, \beta_{23}, \beta_{31}$ interaction coefficients and A, B, C are the independent variables studied.

The predicted values of % were obtained by substituting the values of the parameters considered from Table 4 into Eq. 2.

$$Y_1 = 92.6 + 0.37A - 13.26B + 3.44C + 0.22AB - 0.1AC + 1.72BC - 3.74A^2 - 3.04B^2 - 4.27C^2 \qquad (2)$$

The designed experiments along with experimental and predicted values of the two responses are shown in Table 4.

The actual and the predicated values of degradation are in agreement with each other. Moreover, It is found that at pH = 7, the highest amount of MBO (~ 90.50) is photodegraded by ZnO/HPA nanophotocatalyst. These results further are consistent with Fig. 6b findings.

Effect of ZnO/HAP loading

To obtain the optimum dosage of ZnO/HAP, a series of experiments were carried using various amounts of nanophotocatalyst, from 10 to 200 mg L^{-1}, in the solution of MBO (Fig. 6b). The results demonstrated that the rate of photodestruction of MBO increase linearly with ZnO/HAP loading up to 50 mg L^{-1}. This is attributed to the high number of active sites on photocatalyst surface which in
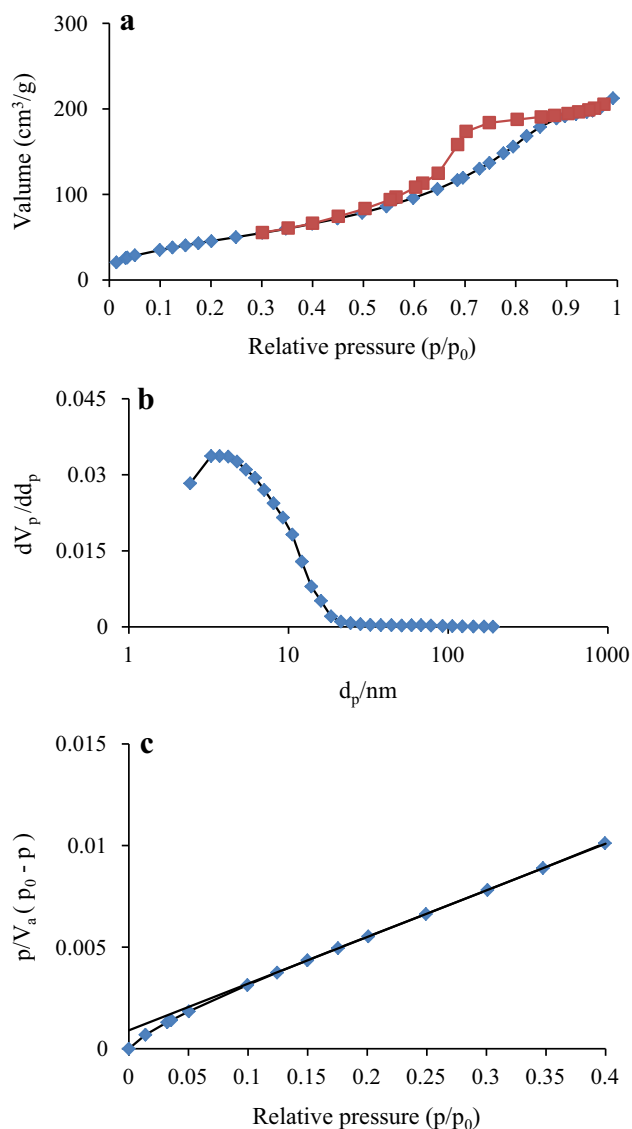
Fig. 5 **a** N₂ adsorption–desorption isotherm, **b** pore size distribution curves, and **c** BET plot of ZnO/HAP nanocomposite

Table 1 BET surface characteristics of the ZnO/HAP and pure ZnO nanoparticles

Nanoadsorbent	BET (mg^2g^{-1})	Pore volume (cm^3g^{-1})	Pore size (nm)	Reference
ZnO/HAP	182.36	0.0329	7.182	This work
Pure ZnO	31.2	0.12	15.81	Georgekutty et al. (2008)

turn increase the amount of hydroxyl and superoxide radicals (Bandekar et al. 2014). Above this loading, increase in turbidity of the solution reduces the UV light penetration throughout the solution (Hameed et al. 2011). Accordingly,

Table 2 Comparison of photocatalytic activity of nanoadsorbents on degradation rate of MBO

Nanoadsorbent	Removal %	Reference
ZnO/HAP	99.45	This work
ZnO	50.8	This work
HAP	41.8	This work

degradation rate of MBO by nanocomposite would diminish. Therefore, an optimal dosage of ZnO/HAP photocatalysts for the degradation of MBO was adjusted at 50 mg L^{-1}.
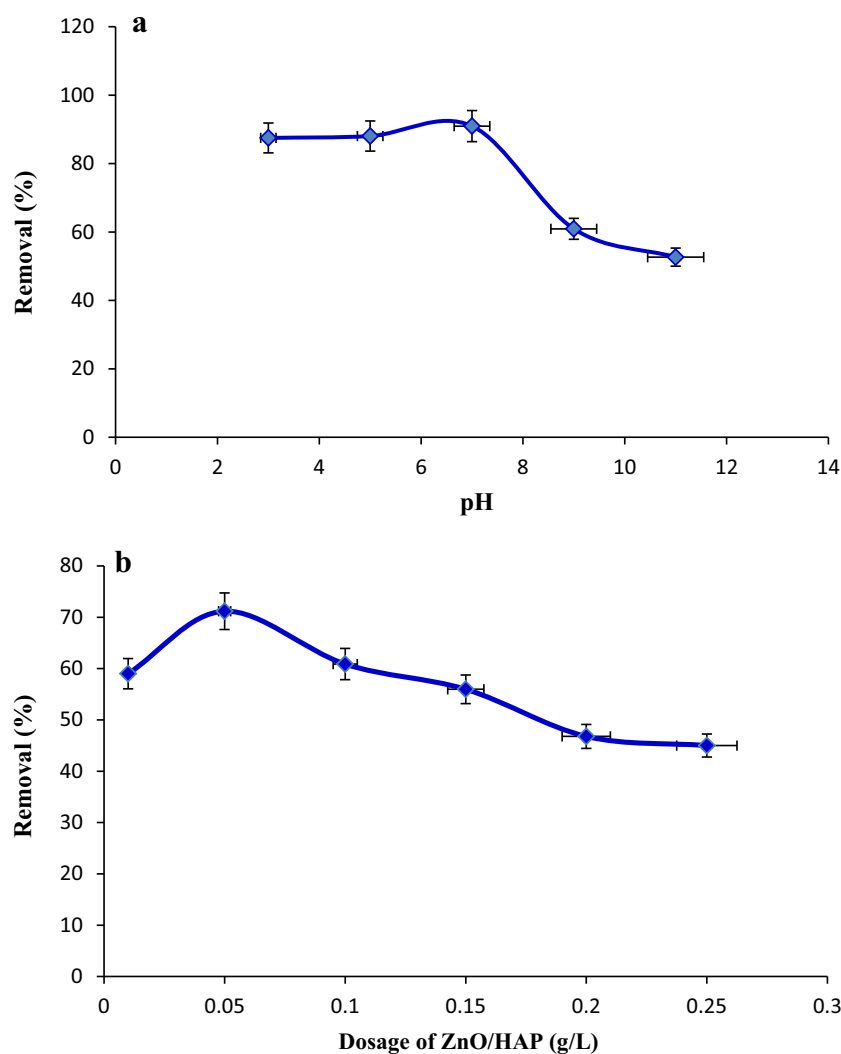
Effect of initial concentration of MBO

In order to investigate the effect of initial concentration of MBO on the photocatalytic degradation efficiency of ZnO/HAP, an experiment was carried out by varying the initial concentration of MBO from 10 to 100 mg L^{-1} at pH = 7 and room temperature (25 °C) (Fig. A1). The results depicted that the highest rate of degradation of MBO was achieved at the optimal initial concentration of 20 mg L^{-1}. Beyond this value, the rate of degradation of MBO considerably decreases. It was assumed that at higher concentration, there are a fewer active sites on the nanoadsorbent surface, hence, the hydroxyl and oxygen radicals attacking the MBO molecules decrease with increase in concentration of MBO (Sakthivel et al. 2003). Moreover, the Figs. 6b, A1 results further were confirmed by correlation graph of removal of MBO and optimal ratio of catalyst loading/MBO (Fig. 7). Evidently there is good linear correlation between optimal ratio of catalyst loading/MBO and removal efficiency of MBO pollutant. Approximately, at catalyst loading/MBO = 200 the highest value of MBO is photo-eliminated. These results indicated that fewer values of both ZnO/HAP nanocatalyst and MBO pollutant highly influence the removal efficiency of MBO in solution. These observations are in agreement with Figs. 6b and A1 results.

Effect of irradiation time

Figure 8 represents the relationship between the removal of MBO with the irradiation time using ZnO/HAP nanophotocatalyst. It was found that the rate of MBO degradation considerably increases with increase in irradiation time, so that the concentration of MBO was reduced to more than 85 % within 2 h. Apparently, with increase in irradiation time, the formation of strong $HO^\bullet$ and $O_2^{-2\bullet}$ radicals increases and thus by breaking different bonds in the MBO

Fig. 6 **a** Effect of various solution pH and **b** effect of the ZnO/HAP loading on the degradation of MBO (initial concentration: 20 mg L^{-1}, irradiation time: 2 h and 25 mL solution of MBO)

Table 3 The levels and ranges of variables in Box–Behnken statistical experiment design

Independent variables	Symbol	Coded variable level		
		Low −1	Center 0	High +1
Catalytic dose (g L^{-1})	A	0.01	0.05	0.1
Initial concentration of MBO (ppm)	B	10	20	40
pH	C	5	7	9

molecule, lead to its full degradation in the course of time (Elmolla and Chaudhuri 2010; Hayat et al. 2011; Tian et al. 2012).

Effect of initial concentration of MBO on absorption capacity of ZnO/HAP

The absorption capacity of adsorbent was determined under optimized conditions (pH = 7, irradiation time = 120 min, stirring speed = 400 rpm) by batch method (Parham et al. 2012). 50 mg of ZnO/HAP nanophotocatalyst was added to a 25-mL solution containing 20 mg L^{-1} of MBO and stirred for 1 h. Removal percent and adsorbed amount of MBO was probed by cold vapor atomic absorption measurement of the sample solution before and after removing process. The adsorption capacity of ZnO/HAP was calculated using the following equation:

$$q_e = \frac{(c_0 - c_t)V}{M} \tag{3}$$

where q_e is the amount of MBO adsorbed on the ZnO/HAP (mg g^{-1}), C_0 and C_t are concentration of MBO in solution before and after adsorption (mg L^{-1}), V is the volume (L) and M is the amount of the ZnO/HAP used in the reaction. The loading capacity of nanocomposite was determined to be about 198 mg g^{-1}. It was found that with increasing concentration of MBO, the absorption rate is increased accordingly (Fig. A2).

Table 4 Box–Behnken experiments along with actual and predicted values of responses

| MBO removal (%)					
Run	Catalytic dose (g L^{-1})	Initial concentration of MBO (ppm)	pH	Actual	Predicted
1	0.01	10	7	85.20	85.92
2	0.1	10	7	85.36	85.22
3	0.01	40	7	71.83	71.97
4	0.1	40	7	72.87	73.15
5	0.01	20	5	80.45	80.68
6	0.1	20	5	81.52	81.62
7	0.01	20	9	83.85	87.76
8	0.1	20	9	83.52	88.29
9	0.05	10	5	79.78	76.83
10	0.05	40	5	79.25	66.88
11	0.05	10	9	69.89	70.00
12	0.05	40	9	57.24	57.19
13	0.05	20	7	90.53	90.60
14	0.05	20	7	90.82	90.60
15	0.05	20	7	90.44	90.60

Photocatalytic mechanism

Figure 9 elucidates the mechanism of photocatalytic oxidation of MBO using ZnO/HAP nanophotocatalyst. After immobilizing ZnO Nps on the surface of HAP, the latter, being major contributor to the photodegradation of MBO. On the other hand, after modifying ZnO by HAP, the SSA and the concentration of hydroxyl groups considerably increase. In a typical photocatalytic reaction,

photogenerating electrons and holes are captured by O_2 and H_2O absorbed by ZnO forming superactive $^{\bullet}OH$ and O_2^{-} oxidants. Hence, the enhanced photodegradation of MBO can be promoted by the increase in the concentration of surface hydroxyl groups and molecular oxygen. Accordingly, the increase in amount of hydroxyl not only increases the trapping sites for photogenerated holes, but also can increase the trapping sites for photogenerated electrons by adsorbing more molecular oxygen, resulting in more hydroxyl radicals to participate in the photocatalytic reaction. Consequently, ZnO/HAP exhibited the highest photocatalytic activity than all the other reported nanophotocatalysts (Fig. 9) (Mohamed and Aazam; Sakthivel et al. 2003).

Comparison of photocatalytic activity of ZnO/HAP with ZnO and HAP nanoparticles

In order to evaluate the efficiency of ZnO/HAP nanophotocatalyst, identical experiments were also carried out with ZnO, and HAP nanoparticles on the photocatalytic degradation of MBO and the results were illustrated in Table 2. Evidently, the results indicated that the highest removal efficiency of MBO (99.45 %) occurred by ZnO/HAP using UV light as energy source. The trend of photocatalytic activity of our studied nanophotocatalysts for degradation of MBO was ZnO/HAP > ZnO > HAP (Table 2). Obviously, doping ZnO in HAP matrix was expected to enhance the surface area, hydroxyl radicals species and improve photocatalytic performance of ZnO/HAP rather than pure ZnO and HAP Nps (see Table 1) (Giannakopoulou et al. 2012; Sakthivel et al. 2003).
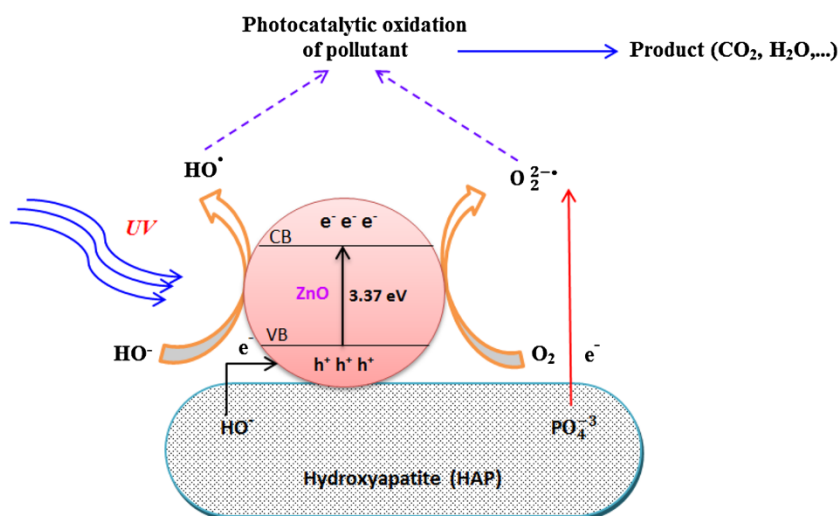
Fig. 7 The correlation between photodegradation of MBO and optimal ratio of ZnO/HAP loading and the initial MBO concentration
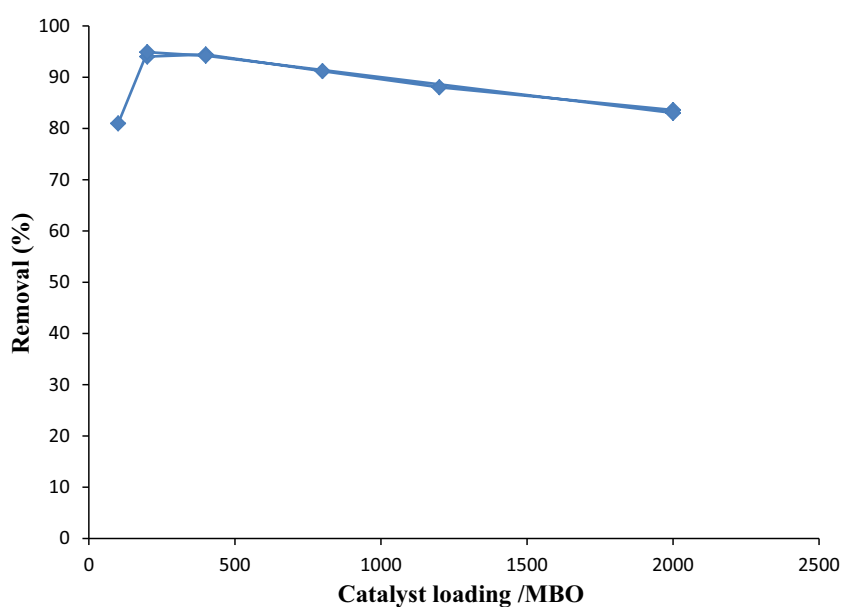
Fig. 8 Effect of irradiation time on degradation of MBO using ZnO/HAP (initial concentration: 20 mg L^{-1}, pH 7, and 25 mL solution of MBO)
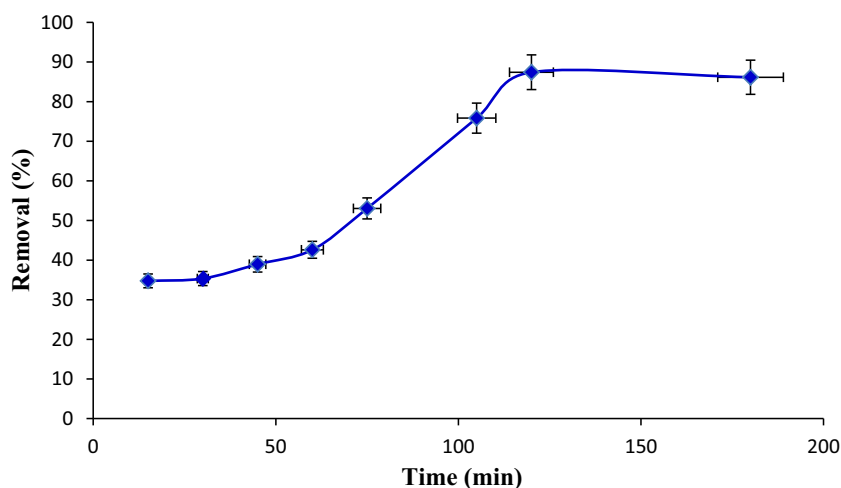
Fig. 9 Proposed photocatalytic mechanism of MBO by ZnO/HAP nanocomposite

Conclusions

The ZnO/HAP nanocomposite with high photocatalytic activities was observed to be an efficient photocatalyst for degradation of odorous MBO in water. The chemical composition, morphology, size, phase structure and specific surface area of ZnO/HAP are characterized by FTIR, TEM, XRD, SEM, and BET techniques, respectively. The results showed that MBO was completely photodegraded within 120 min by ZnO/HAP at the optimum conditions: pH = 7, adsorbent loading = 50 mg and initial concentration of MBO = 20 mg L^{-1}. The results demonstrated that photodecomposition of MBO on ZnO/HAP surface was much faster than pure ZnO and HAP Nps using UV light as source energy. It is hoped that our prepared ZnO/HAP nanophotocatalyst with higher specific surface areas offers superior photoreaction procedure for organic pollutants decomposition.

References

Ali I (2012) New generation adsorbents for water treatment. Chem Rev 112:5073–5091

Allaouia AMM, Wong-Wah-Chung P (2010) Homogeneous photodegradation study of 2-mercaptobenzothiazole photocatalysed by sodium decatungstate salts: kinetics and mechanistic pathways. J Photochem Photobiol A Chem 212:153–160

Amer W et al (2014) Microwave-assisted synthesis of mesoporous nano-hydroxyapatite using surfactant templates. CrystEngComm 16:543–549

Antonopoulou M, Evgenidou E, Lambropoulou D, Konstantinou I (2014) A review on advanced oxidation processes for the

removal of taste and odor compounds from aqueous media. Water Res 53:215–234

Azzaoui K et al (2014) Synthesis and characterization of composite based on cellulose acetate and hydroxyapatite application to the absorption of harmful substances. Carbohydr Polym 111:41–46

Bahnemann DW (1991) Mechanisms of organic transformations on semiconductor particles. Photochemical conversion and storage of solar energy. Kluwer Academic Publishers, The Netherlands

Bai X, Wang L, Zong R, Lv Y, Sun Y, Zhu Y (2013) Performance enhancement of ZnO photocatalyst via synergic effect of surface oxygen defect and graphene hybridization. Langmuir 29:3097–3105

Bandekar G, Rajurkar N, Mulla I, Mulik U, Amalnerkar D, Adhyapak P (2014) Synthesis, characterization and photocatalytic activity of PVP stabilized ZnO and modified ZnO nanostructures. Appl Nanosci 4:199–208

Birks L, Friedman H (2004) Particle size determination from X-ray line broadening. J Appl Phys 17:687–692

Bouyarmane H, Saoiabi S, Laghzizil A, Saoiabi A, Rami A, El Karbane M (2013) Natural phosphate and its derivative porous hydroxyapatite for the removal of toxic organic chemicals. Desalin Water Treat 1–5. doi:10.1080/19443994.2013.831797

Buazar F, Cheshmehkani A, Kassaee M (2012) Nanosteel synthesis via arc discharge: media and current effects. J Iran Chem Soc 9:151–156

Chong MN, Jin B, Chow CW, Saint C (2010) Recent developments in photocatalytic water treatment technology: a review. Water Res 44:2997–3027

Deng Z, Chen M, Gu G, Wu L (2008) A facile method to fabricate ZnO hollow spheres and their photocatalytic property. J Phys Chem B 112:16–22

Elmolla ES, Chaudhuri M (2010) Degradation of amoxicillin, ampicillin and cloxacillin antibiotics in aqueous solution by the UV/ZnO photocatalytic process. J Hazard Mater 173:445–449

Georgekutty R, Seery MK, Pillai SC (2008) A highly efficient Ag-ZnO photocatalyst: synthesis, properties, and mechanism. J Phys Chem C 112:13563–13570

Giannakopoulou T, Todorova N, Romanos G, Vaimakis T, Dillert R, Bahnemann D, Trapalis C (2012) Composite hydroxyapatite/TiO$_2$ materials for photocatalytic oxidation of NO$_x$. Mater Sci Eng B 177:1046–1052

Greyson JC (1990) Carbon, nitrogen, and sulfur pollutants and their determination in air and water. CRC Press, USA

Habibi MH, Sheibani R (2010) Photocatalytic oxidation of four model mercaptans from aquatic environment using Ag-ZnO nanocomposite thin film for odor control. J Adv Oxid Technol 13:192–199

Habibi MH, Sheibani R (2012) Removal of 2-mercaptobenzoxazole from water as model of odorous mercaptan compounds by a heterogenous photocatalytic process using Ag-ZnO nanocomposite coated thin film on glass plate. Bull Environ Contam Toxicol 85:589–592

Hameed B, Akpan U, Wee KP (2011) Photocatalytic degradation of acid red 1 dye using ZnO catalyst in the presence and absence of silver. Desalin Water Treat 27:204–209

Hariharan C (2006) Photocatalytic degradation of organic contaminants in water by ZnO nanoparticles: revisited. Appl Catal A 304:55–61

Hayat K, Gondal M, Khaled MM, Ahmed S, Shemsi AM (2011) Nano ZnO synthesis by modified sol gel method and its application in heterogeneous photocatalytic removal of phenol from water. Appl Catal A 393:122–129

Hokkanen S, Repo E, Westholm LJ, Lou S, Sainio T, Sillanpää M (2014) Adsorption of Ni^{2+}, Cd^{2+}, PO$_4^{3-}$ and NO$_3^-$ from aqueous solutions by nanostructured microfibrillated cellulose modified with carbonated hydroxyapatite. Chem Eng J 252:64–74

Kassaee M, Buazar F (2009) Al nanoparticles: impact of media and current on the arc fabrication. J Manuf Process 11:31–37

Kassaee M, Motamedi E, Majdi M, Cheshmehkani A, Soleimani-Amiri S, Buazar F (2008) Media effects on nanobrass arc fabrications. J Alloys Compd 453:229–232

Leh F, Chan K (1973) Sulfur compounds. Pollution, health effects, and biological function. J Chem Educ 50:246

Liu JX, Wang F, Shen JX, Lai QH, Gai Y (2013) Study of nano-hydroxyapatite adsorption in heavy metals. Adv Mater Res 777:15–18

Mahdavi S, Jalali M, Afkhami A (2012) Removal of heavy metals from aqueous solutions using Fe3O4, ZnO, and CuO nanoparticles. J Nanopart Res 14:1–18

Mohamed R, Aazam E (2013) Synthesis and characterization of Pt–ZnO-hydroxyapatite nanoparticles for photocatalytic degradation of benzene under visible light. Desalin Water Treat 51:6082–6090

Mohammad Vaseem AU, Yoon-Bong Hahn (2010) ZnO Nanoparticles: Growth, Properties, and Applications. In: Umar A (ed) Metal Oxide Nanostructures and Their Applications, vol 5. American Scientific Publishers, USA, pp 1–36

Neppolian B, Sakthivel S, Arabindoo B, Palanichamy M, Murugesan V (1998) Photocatalytic degradation of textile dye commonly used in cotton fabrics. Stud Surf Sci Catal 113:329–335

Parham H, Khoshnam F (2013) Highly efficient and simultaneous removal of 2-mercaptobenzothiazole and 2-mercaptobenzoxazole from water samples by copper oxide nanoparticles. J Chem Technol Biotechnol 88:1736–1743

Parham H, Zargar B, Shiralipour R (2012) Fast and efficient removal of mercury from water samples using magnetic iron oxide nanoparticles modified with 2-mercaptobenzothiazole. J Hazard Mater 205:94–100

Sakthivel S, Neppolian B, Shankar M, Arabindoo B, Palanichamy M, Murugesan V (2003) Solar photocatalytic degradation of azo dye: comparison of photocatalytic efficiency of ZnO and TiO$_2$. Sol Energy Mater Sol Cells 77:65–82

Saravanan R, Karthikeyan S, Gupta V, Sekaran G, Narayanan V, Stephen A (2013) Enhanced photocatalytic activity of ZnO/CuO nanocomposite for the degradation of textile dye on visible light illumination. Mater Sci Eng C 33:91–98

Sheela T, Nayaka YA, Viswanatha R, Basavanna S, Venkatesha T (2012) Kinetics and thermodynamics studies on the adsorption of Zn (II), Cd (II) and Hg(II) from aqueous solution using zinc oxide nanoparticles. Powder Technol 217:163–170

Tian C, Zhang Q, Wu A, Jiang M, Liang Z, Jiang B, Fu H (2012) Cost-effective large-scale synthesis of ZnO photocatalyst with excellent performance for dye photodegradation Chem Commun 48:2858–2860

Wei W, Sun R, Jin Z, Cui J, Wei Z (2014) Hydroxyapatite–gelatin nanocomposite as a novel adsorbent for nitrobenzene removal from aqueous solution. Appl Surf Sci 292:1020–1029

Xie J et al (2013) Preparation of titania/hydroxyapatite (TiO$_2$/HAp) composite photocatalyst with mosaic structure for degradation of pentachlorophenol. Mater Lett 110:57–60

Yusoff N, Ong S-A, Ho L-N, Wong Y-S, Khalik W (2014) Degradation of phenol through solar-photocatalytic treatment by zinc oxide in aqueous solution. Desalin Water Treat 1–8. doi:10.1080/19443994.2014.908414

Zhang J, Fu D, Xu Y, Liu C (2010) Optimization of parameters on photocatalytic degradation of chloramphenicol using TiO$_2$ as photocatalyst by response surface methodology. J Environ Sci 22:1281–1289

Zhang G, Shen X, Yang Y (2011) Facile synthesis of monodisperse porous ZnO spheres by a soluble starch-assisted method and their photocatalytic activity. J Phys Chem C 115:7145–7152

Zhao X-Y, Zhu Y-J, Lu B-Q, Chen F, Qi C, Zhao J, Wu J (2014a) Hydrothermal synthesis of hydroxyapatite nanorods using pyridoxal-5′-phosphate as a phosphorus source. Mater Res Bull 55:67–70

Zhao X-Y, Zhu Y-J, Zhao J, Lu B-Q, Chen F, Qi C, Wu J (2014b) Hydroxyapatite nanosheet-assembled microspheres: hemoglobin-templated synthesis and adsorption for heavy metal ions. J Colloid Interface Sci 416:11–18